The spectrum of arsenic hydride: An ab initio configuration interaction study employing a relativistic effective core potential

Aleksey B. Alekseyev, Heinz-Peter Liebermann, Gerhard Hirsch, and Robert J. Buenker

Citation: The Journal of Chemical Physics **108**, 2028 (1998); doi: 10.1063/1.475582
View online: http://dx.doi.org/10.1063/1.475582
View Table of Contents: http://scitation.aip.org/content/aip/journal/jcp/108/5?ver=pdfcov
Published by the AIP Publishing

The spectrum of arsenic hydride: An *ab initio* configuration interaction study employing a relativistic effective core potential

Aleksey B. Alekseyev, Heinz-Peter Liebermann, Gerhard Hirsch, and Robert J. Buenker[a)]
Bergische Universität-Gesamthochschule Wuppertal, Fachbereich 9-Theoretische Chemie, Gaußstr. 20, D-42097 Wuppertal, Germany

(Received 9 September 1997; accepted 20 October 1997)

An *ab initio* configuration interaction (CI) study including the spin–orbit interaction is carried out for numerous valence and Rydberg states of the AsH radical by employing a relativistic effective core potential for the arsenic atom. The computed spectroscopic constants are in good agreement with corresponding experimental data, with a tendency toward a slight overestimation of bond lengths (by 0.01–0.02 Å) and T_e values (by 450–550 cm^{-1}) for the lowest singlet states. Measured spin–orbit splittings for the $X\ ^3\Sigma^-$ and $A\ ^3\Pi$ multiplets are also accurately reproduced in the present calculations and the $\Omega=0^-$, 1, and 2 components of the latter state are shown to be strongly predissociated due to spin–orbit interaction with the corresponding components of the repulsive $^5\Sigma^-$ state. Dipole moments $\mu(v=0)$ for the lowest-lying $X\ ^3\Sigma^-$, $a\ ^1\Delta$, and $b\ ^1\Sigma^+$ states, all arising from the $\cdots\sigma^2\pi^2$ electronic configuration, are computed to have small (e.g., 0.1266 D for $X_1\ ^3\Sigma^-_{0+}$) and nearly equal positive values (As^-H^+ polarity). This finding is used to explain why the partial radiative lifetime for the parallel $b-X_1$ transition ($\tau_p=44$ ms) is much longer than that ($\tau_p=0.95$ ms) of the perpendicular $b-X_2$. The lifetime of the $a\ ^1\Delta$ state is calculated to be 97 ms, significantly longer than that of the $b\ ^1\Sigma^+$ state, while the $A\ ^3\Pi$ substates have much shorter lifetimes ($\leqslant 1\ \mu$s) for radiative decay to the $X\ ^3\Sigma^-$ ground state. A number of other bound states and avoided crossings are indicated in the calculations which may be of relevance in future experimental studies of this system. © *1998 American Institute of Physics.* [S0021-9606(98)00305-5]

I. INTRODUCTION

Recently Beutel *et al.*[1] have observed the $a\ ^1\Delta-X\ ^3\Sigma^-$ infrared emission spectrum of AsH and determined spectroscopic constants for the upper state involved in this transition. Thus they have completed the characterization of the low-energy electronic spectrum of the AsH radical, which belongs to the wide class of systems with an $X\ ^3\Sigma^-$ ground and $a\ ^1\Delta$, $b\ ^1\Sigma^+$ excited states, all having the same $\cdots\sigma^2\pi^2$ electronic configuration. Another common feature of such systems is the low-lying $A\ ^3\Pi$ state, which arises in this case from the $\sigma\rightarrow\pi$ electron excitation and is connected with the $X\ ^3\Sigma^-$ ground state by a spin- and symmetry-allowed transition, which therefore is anticipated to be fairly strong. It was indeed the first AsH transition to be observed, and was found by Dixon *et al.*[2,3] in the UV absorption spectra during the flash photolysis of arsine (AsH_3). Though these authors were able to identify all four components of the $A\ ^3\Pi$ multiplet in the recorded spectra, spectroscopic constants determined in this study for the A state are considered to be approximate due to the fact that only the 0–0 and 1–0 (for AsD) vibrational bands were detected and large perturbations of the A state were observed.

Subsequent experimental studies of AsH concentrated mainly on the refinement of spectroscopic data for the spin–split $X\ ^3\Sigma^-$ ground state,[4–6] as well as on the low-lying metastable $b\ ^1\Sigma^+$ and $a\ ^1\Delta$ states.[1,7] Kawaguchi and Hirota[4] have observed the far-infrared laser magnetic resonance (LMR) spectrum of AsH in the $X\ ^3\Sigma^-$ state and determined its rotational, fine structure and hyperfine coupling constants. Anacona *et al.*[5] provided the first results for the $X\ ^3\Sigma^-$ excited vibrational levels by means of IR (infrared) diode laser spectroscopy. Hensel *et al.*[6] employed the LMR method to detect for the first time the $\Delta\Omega=\pm1$ transition in the $X\ ^3\Sigma^-$ state and improved the quality of its spectroscopic parameters. Arens and Richter[7] have observed the $b\ ^1\Sigma^+-X\ ^3\Sigma^-$ transition of AsH in emission and determined spectroscopic constants for the $b\ ^1\Sigma^+$ state. In addition, Berkowitz[8] has measured the adiabatic ionization potential of AsH to be 9.641 eV, combined his experimental data with the AsH_3 heat of atomization and determined the AsH dissociation energy D_0 to be 2.80 ± 0.03 eV.

The AsH radical has also attracted fairly strong attention from theoreticians.[9–12] The first *ab initio* study of this system was carried out by Pettersson and Langhoff,[9] who calculated spectroscopic constants and a dipole moment for the $X\ ^3\Sigma^-$ ground state. These calculations were performed at a quite high level of correlation treatment, including the $3d$ shell of As, but without inclusion of relativistic effects, neither scalar (mass-velocity and Darwin corrections) nor spin–orbit. The influence of such effects on the electronic structure of AsH has been investigated by Matsushita *et al.*[10] who were the first to carry out large-scale multireference through double excitation configuration interaction (MRD-CI) calculations to study the low-lying valence and Rydberg states of this radical. The spin–orbit interaction has been included in their

[a)]Present address: Department of Chemistry, North Carolina State University, Raleigh, North Carolina 27695-8204.

treatment by means of a variational perturbation procedure in order to calculate zero-field splittings of the $X\ ^3\Sigma^-$ and $A\ ^3\Pi$ states and to estimate transition moments and corresponding lifetimes for transitions between the lowest three states of AsH at the ground-state equilibrium distance. In the above two studies all electrons were included in the calculations explicitly, whereas Balasubramanian *et al.*[11,12] have employed a relativistic effective core potential (RECP) for the As atom to investigate this radical. In the first of these studies[11] the r_e and D_e values for the AsH ground state were calculated, while in the second[12] potential-energy curves and spectroscopic constants for sixteen low-lying electronic states of AsH were obtained at the $\Lambda-S$ level of treatment, i.e., without including spin–orbit coupling. Eleven of these states were found to be bound and possible radiative transitions between them discussed.

Although one can conclude from the above discussion that the AsH electronic structure is quite well investigated to date and the overall agreement of the *ab initio* calculated and experimental results may be considered to be fairly good, there are still a number of interesting questions to be answered. In particular, the recent spectroscopic investigations of the $a\ ^1\Delta$ and $b\ ^1\Sigma^+$ states[1,7] have shown that the measured excitation energies are quite strongly overestimated (by about $1000-3000\ \mathrm{cm}^{-1}$) in the *ab initio* calculations of both all-electron[10] and core-potential[12] type, and this in turn should noticeably influence the calculated values of transition probabilities for these states. It is also worth noting that the spin–orbit (SO) interaction has not been included in any of the previous studies to compute potential energy curves in the whole range of internuclear distances. Although the SO coupling is not expected to strongly influence the r_e and ω_e values of the AsH states, it is very important for the accurate calculation of excitation energies as well as of radiative lifetimes and avoided crossings of electronic states.

The main objective of the present study is thus to carry out systematic calculations of potential-energy curves, transition moments, and radiative lifetimes for the valence and Rydberg states of AsH within a computational scheme which consistently includes spin–orbit coupling. For this purpose a relativistic CI approach is employed which has been recently developed in our laboratory and is based on RECPs. Similar calculations have recently been carried out for the isovalent BiH radical[13] as well as for As atom-containing diatomics such as AsF[14] and AsO,[15] and comparison with available experimental data has shown that they are able to provide a reliable description of the electronic structure of these systems. The present study also has the specific goal of theoretically predicting excited AsH states which are connected with the $a\ ^1\Delta$ state by fairly strong transitions. Such information may be very useful for future experimental studies of the kinetic properties of the metastable $a\ ^1\Delta$ state in chemical reactions and energy transfer processes. The $a\ ^1\Delta$ state population in such processes may be controlled experimentally by means of laser excitation to some higher-lying electronic state and observation of emission from it to the ground state. This method is preferable to direct observation of the $a\ ^1\Delta-X\ ^3\Sigma^-$ emission because of the weakness of the latter transition. An obvious candidate for the upper state in the above scheme is the first $\sigma\rightarrow\pi\ ^1\Pi$. The analogous $c\ ^1\Pi$ state in the NH radical is known to be bound, and Balasubramanian and Nannegari[12] have also calculated it to be bound in AsH, though it has never been observed experimentally. We will therefore give special attention to the question of whether this $^1\Pi$ state can really serve as the upper state in the above experimental scheme, and also check other candidates for this role such as the $A\ ^3\Pi_{1,2}$ spin components to which transitions from the $a\ ^1\Delta$ become allowed due to the fairly strong spin–orbit coupling in AsH.

The structure of the present paper is the following. In Sec. II the method employed is briefly described. Section III considers the results calculated at the $\Lambda-S$ level, i.e., without including SO coupling, while Sec. IV presents potential-energy curves and spectroscopic constants for the final Ω states. Computed transition moments, radiative lifetimes and dipole moments are then considered before summarizing the main conclusions in Sec. VI.

II. DETAILS OF THE THEORETICAL TREATMENT

In the present theoretical treatment the core electrons of the arsenic atom are described by a RECP given by Hurley *et al.*[16] with only the $4s$ and $4p$ electrons treated explicitly via basis functions. Experience with our previous calculations of AsF[14] and AsO[15] employing the same RECP shows that it may lead to a small (0.01–0.02 Å) overestimation of equilibrium distances due to to the lack of the As $3d$ shell polarization. This effect should be approximately the same for all low-lying states of AsH, however, since excitations out of the $3d$ shell are not expected to play any important role in their electronic structure, and thus should not influence the relative position of these states. This view is also supported by the calculations of Pettersson and Langhoff,[9] who found that correlating the $3d$ electrons at the coupled pair functional (CPF) level resulted in a small (0.01–0.02 Å) decrease in r_e for the AsH ground state. On the other hand, employing a full-core RECP means that only six electrons of AsH are considered explicitly and that this can be done at a very high level of correlation treatment which is critical for obtaining accurate excitation energies for states of different multiplicities.

The $3s3p$ AO Cartesian Gaussian basis set recommended for use with the As RECP on the basis of SCF optimization[16] has been taken as a starting point in the present study but has been reoptimized for the As atomic $^4S°$ ground state at the CI level. The exponents thus obtained are 1.20, 0.32, and 0.18 a_0^{-2}, and 1.976, 0.33, and 0.1024 a_0^{-2} for the three s and three p basis functions, respectively, and differ only slightly from the original ones.[16] This AO basis set has been augmented by two d (0.32 and 0.10 a_0^{-2}) and two f (0.42 and 0.10 a_0^{-2}) functions, also optimized in the $^4S°$ state calculations. It was also necessary to add diffuse $s(0.012\ a_0^{-2})$ and $p(0.015\ a_0^{-2})$ functions to describe low-lying Rydberg states in the AsH spectrum, so that the final basis set for the As atom consists of $4s4p2d2f$ functions employed in uncontracted form. The corresponding basis set

TABLE I. Excitation energies (in cm^{-1}) of the lowest-lying states of the As atom obtained in the present RECP calculation with SO coupling in comparison with experimental data (Ref. 18).

Config.	Design.	J	Calc.	Expt.
$4s^24p^3$	$^4S°$	3/2	0	0
$4s^24p^3$	$^2D°$	3/2	11 217	10 593
		5/2	11 519	10 915
$4s^24p^3$	$^2P°$	1/2	19 015	18 186
		3/2	19 416	18 648
$4s^24p^25s^1$	^4P	1/2	50 955	50 964
		3/2	51 271	51 610
		5/2	52 998	52 898

for the hydrogen atom is the same as used earlier in our BiH study,[13] i.e., the $5s$ primitive set of Dunning[17] contracted to $3s$ and augmented by a single p function with exponent of 1.0 a_0^{-2}.

Before carrying out molecular calculations the same RECP and AO basis have also been employed for the As atomic tests to compare with the corresponding experimental data[18] and the calculated results of Balasubramanian and Nannegari.[12] The excitation energy values for the four lowest $L-S$ states are summarized in Table I. One can see that a fairly high level of correlation treatment is achieved in the present study, though there is still an overestimation of the excitation energy for the $^2D°$ and $^2P°$ states by about 600 and 800 cm^{-1}, respectively. This is not very surprising since it is well known that it is difficult to correlate states of low multiplicity with the same accuracy as those of higher spin, in this case doublets in comparison with the quartet ground state. The accuracy is considerably improved, relative to the 2000–2600 cm^{-1} overestimation obtained in Ref. 12, however, and one can anticipate that approximately the same level of accuracy should be achieved for the $a\ ^1\Delta$ and $b\ ^1\Sigma^+$ states of AsH, which converge to the As $^2D°$ and $^2P°$ atomic limits, respectively. A noticeably higher level of accuracy is obtained for the lowest ^4P $(4p\rightarrow 5s)$ Rydberg state, as is expected for a quartet state. Table I also shows quite good agreement between the calculated and experimental spin–orbit splittings for the $^2D°$, $^2P°$, and ^4P states of As, with a small tendency to underestimate them in the present study.

The first step in the theoretical treatment of the AsH radical is an SCF (self-consistent field) calculation of the $^3\Sigma^-$ $(\sigma^2\pi^2)$ ground state. The resulting SCF-MOs (self-consistent field molecular orbital) are then used as orthonormal basis for the ensuing CI calculations. These orbitals transform according to linear group irreducible representations, but the computations are carried out in formal C_{2v} symmetry in order to take advantage of the simplicity of the abelian group direct product relationships. The conventional multireference single- and double-excitation (MRD-CI) method[19] is employed to obtain a rather large number of roots (up to eight) of various $\Lambda-S$ symmetries, from singlets through quintets. At this stage of the calculations the SO interaction is neglected, but other relativistic effects are included through the spin-independent part of the As RECP. Results are obtained at 55 internuclear distances, ranging from 1.6 to 10.0 a_0, with an increment of 0.05 a_0 in the neighborhood of the ground-state equilibrium distance (2.6–3.2 a_0) and important avoided crossings (4.1, 4.9 a_0), a standard increment of 0.1 a_0 up to 5.5 a_0 and at selected points beyond this distance. A number of key reference configurations is chosen for each of the low-lying AsH roots on the basis of the absolute magnitudes of their associated coefficients in the final CI wave functions at different distances, and these reference sets are used for each $\Lambda-S$ symmetry for the whole range of internuclear separations considered in order to obtain smooth potential curves at approximately the same level of accuracy. A perturbative selection procedure is employed to reduce the sizes of the secular equations solved in each case. Energy results at the unselected level of treatment $(T\rightarrow 0)$ are then obtained by an extrapolation procedure,[19] while the effects of higher excitations (estimated full CI energies) are taken into account via a generalization of the Davidson correction.[20,21] Details concerning the sizes of secular equations treated may be found in Table II as well as the numbers and symmetries of the roots obtained. The linear notation for the lowest two roots in each C_{2v} space is also given, along with the sums of squared coefficients of reference configurations Σc_p^2 in the corresponding final wave functions. The Table CI algorithm[22] is used in the computational scheme in order to deal efficiently with the complicated open-shell relationships which arise among the various pairs of selected configurations.

TABLE II. Technical details of the MRD-CI calculations for the AsH molecule at $T=1\ \mu E_h$.[a]

C_{2v}	$N_{\text{ref}}/N_{\text{root}}$	SAFTOT/SAFSEL	$C_{\infty v}$	Σc_p^2
$^1A_1$	231/8	550 938/22 627	$^1\Delta$	0.9463
			$^1\Sigma^+$	0.9367
$^1A_2$	142/8	500 312/19 060	$^1\Delta$	0.9394
			$^1\Sigma^-$	0.9299
$^1B_{1,2}$	172/8	494 610/23 131	$1\ ^1\Pi_{x,y}$	0.9353
			$2\ ^1\Pi_{x,y}$	0.9377
$^3A_1$	197/8	858 091/27 151	$^3\Delta$	0.9301
			$^3\Sigma^+$	0.9293
$^3A_2$	112/8	720 089/10 366	$^3\Sigma^-$	0.9434
			$^3\Delta$	0.9301
$^3B_{1,2}$	172/8	830 148/28 940	$1\ ^3\Pi_{x,y}$	0.9363
			$2\ ^3\Pi_{x,y}$	0.9384
$^5A_2$	118/2	438 670/8392	$1\ ^5\Sigma^-$	0.9496
			$2\ ^5\Sigma^-$	0.9507
$^5B_{1,2}$	85/2	345 282/7082	$1\ ^5\Pi_{x,y}$	0.9368
			$2\ ^5\Pi_{x,y}$	0.9252

[a]The number of selected SAFs and Σc_p^2 values are given for $r=2.90\ a_0$. SAFTOT designates the total number of generated, SAFSEL the number of selected SAFs. N_{ref} and N_{root} refer to the number of reference configurations and roots treated, respectively.

Using the data from Table II one can compare the present MRD-CI study with the analogous one carried out in Ref. 10. Eight roots have been computed in the present work for each singlet and triplet symmetry, with 85–231 configurations included in the corresponding reference sets, as compared to 4 to 5 roots and 11–37 reference configurations per symmetry in Ref. 10. A selection threshold of $T=1.0\ \mu E_h$ has been employed in the present study instead of

5.0 μE_h,[10] and this leads to CI spaces of 8392–28 940 selected configurations for various symmetries, 4 to 5 times larger than in the previous MRD-CI calculation. So one can conclude that a much more extensive CI treatment is performed in the present study and expect that a noticeably better level of electron correlation may be achieved as a result.

The next step in the present approach is to employ the $\Lambda-S$ eigenfunctions as basis for the final spin–orbit calculations. For this purpose the spatial functions are multiplied with appropriate spin functions and the Wigner–Eckart theorem is employed to compute spin–orbit matrix elements between them based on results obtained for representative pairs of $\mathbf{S}^2$ eigenfunctions. The estimated full CI energies are placed on the diagonal of the Hamiltonian matrices, whereas the variational $\Lambda-S$ wave functions are employed to calculate the off-diagonal spin–orbit matrix elements. The orders of the corresponding secular equations are 34 for A_1 and B_1, and 36 for A_2. Since each B_2 function has a degenerate partner in B_1, it is not necessary to solve both these secular equations explicitly. More details of the theoretical treatment may be found elsewhere.[23]

It is worthwhile to note that in our earlier study of the isovalent BiH radical[13] another approach for the calculation of the final Ω states has been used. In this method the various selected spatial configurations are multiplied with spin functions which transform according to irreducible representations of the C_{2v} double group and the resulting products are grouped together according to symmetry. Spin–orbit matrix elements are then computed between different configuration-state functions (CSFs) and these results are combined with the previous results for the Coulomb and exchange terms to form a full Hamiltonian matrix for each of the four C_{2v} double group representations. The resulting secular equation orders are typically four to six times larger than for the $\Lambda-S$ CI treatments themselves (Table II), depending on how many symmetries and multiplicities are included in the calculation. In other words, all CSFs are allowed in this case to interact by spin–orbit, while in the approach described first, $\Lambda-S$ matrices are diagonalized at the first stage to obtain a limited number of $\Lambda-S$ eigenfunctions, normally 6–10 per symmetry, which are then used in the second step as basis for fairly small spin–orbit calculations to obtain the final Ω states. Our recent atomic tests of both methods[24] have shown that the second procedure can be advantageous for systems with very heavy atoms belonging to the sixth period of the periodic table and beyond, due the fact that high-lying $\Lambda-S$ roots which cannot easily be included in the two-step procedure play a critical role in the formation of the lowest Ω states via the spin–orbit interaction. The method employing the combined CSF basis requires diagonalization of very large matrices, however, and for lighter systems such as the AsH radical considered in the present work, it is preferable to use the two-step method instead since it is less time consuming and provides results of comparable accuracy in this regime, as also shown by the above atomic tests.[24]

The final stage of the present computational scheme involves fitting the resulting potential-energy curves to polynomials which serve as the potentials in one-dimensional nuclear motion Schrödinger equations to be solved numerically.[25,26] The vibrational wave functions obtained are combined with transition moments for the Ω electronic states to compute Einstein coefficients for various pairs of vibrational states, from which the radiative lifetimes of individual upper-state levels are determined by summing over the transition probabilities to all lower-lying states and inverting.

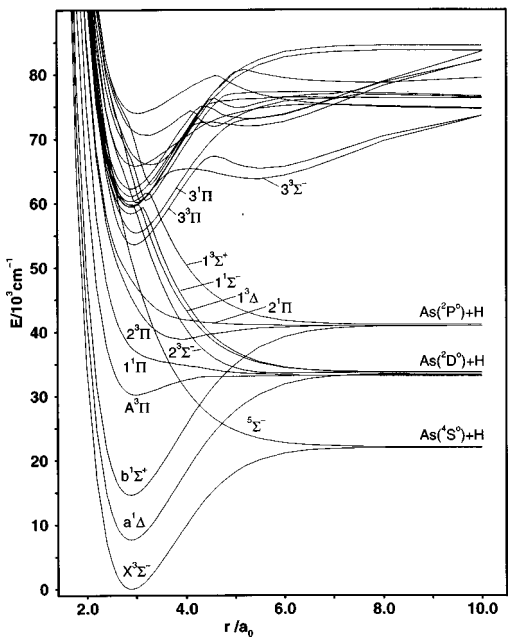

FIG. 1. Computed potential-energy curves of the low-lying $\Lambda-S$ states of AsH obtained without inclusion of the spin–orbit interaction.

III. POTENTIAL-ENERGY RESULTS FOR $\Lambda-S$ STATES

The potential curves obtained from the spin-independent (scalar) CI calculations for the AsH radical are given in Fig. 1. All $\Lambda-S$ molecular states converging adiabatically to the three lowest As atomic states, $^4S°$, $^2D°$, and $^2P°$, in combination with the hydrogenic ground state are shown in this figure, as well as a number of other bound states, mainly Rydberg in nature, going to higher-lying dissociation limits. At short bond distances the most stable electronic configuration is the $\sigma^2\pi^2$ species, producing the familiar series of three multiplets: $X\ ^3\Sigma^- < a\ ^1\Delta < b\ ^1\Sigma^+$. The $X\ ^3\Sigma^-$ state correlates with the $^4S°$ atomic ground state of As, while the $a\ ^1\Delta$ and $b\ ^1\Sigma^+$ converge to $^2D°$ and $^2P°$, respectively. The only other molecular state which correlates with $^4S°$ is the $^5\Sigma^-$ of $\sigma\pi^2\sigma^*$ electronic configuration. It has a repulsive potential curve, which is an indication of the relative strengths of the bonding and antibonding character of the σ and σ^* MOs.

Similar to what was found earlier for BiH,[13] the next most stable states are two pairs of $^{3,1}\Pi$ species, originating from the $\sigma\pi^3$ and $\sigma^2\pi\sigma^*$ configurations. Potential-energy curves for both triplets are bonding, though relatively weakly so, while the singlet potential curves are repulsive (Fig. 1). For the $\sigma\pi^3$ configuration this means that the π MO is con-

siderably less bonding than the σ, which conclusion is consistent with the AO composition of these two orbitals. One can also note that such qualitative behavior for the low-lying $^{3,1}\Pi$ states is typical for the Group VA hydrides, but there exists an important quantitative difference in the strength of the bonding. In the lightest of such systems, NH, both $\sigma\pi^3$ states, $^3\Pi$ and $^1\Pi$, are quite strongly bound, especially the $A\ ^3\Pi$ state, which has a binding energy of ~ 2 eV and is only slightly shifted with respect to the ground state,[27] while in the heaviest of them, BiH, the analogous $^3\Pi$ state has a very shallow minimum strongly shifted to larger distances.[13] This indicates clearly that the σ MO has much more bonding character in the lighter Group VA hydrides. The AsH radical lies in the middle of this group and thus exhibits intermediate properties.

An interesting and instructive comparison can also be made between the Group VA hydrides and halides. In the latter case the lowest pair of $^{3,1}\Pi$ states arises from the $\pi^* \rightarrow \sigma^*$ excitation [the π^* HOMO (highest occupied molecular orbital) in halides corresponds to the π in hydrides] rather than from $\sigma \rightarrow \pi$ as in the hydrides. The explanation is very simple: It is energetically advantageous in the halides to excite an electron from the π^* MO, since it is antibonding for these systems due to the presence of the inner bonding π orbital, which has a strong contribution from the halogen $p_{x,y}$ AOs. An important consequence of this fact is the inverse ordering of the Ω components for the lowest $^3\Pi$ state in the hydrides, as expected for its $\sigma\pi^3$ electronic configuration, which is opposite to that of the lowest $^3\Pi(\sigma^2\pi^*\sigma^*)$ multiplet in the halides.

The other four valence states, $2\ ^3\Sigma^-$, $1\ ^1\Sigma^-$, $1\ ^3\Sigma^+$, and $1\ ^3\Delta$, going to the three lowest dissociation limits, all stem from the the same configuration as $^5\Sigma^-$, namely $\sigma\pi^2\sigma^*$, but avoided crossings with Rydberg states occur at shorter distances and change the character of these states. Altogether eight $\Lambda-S$ states originate from the $\sigma\pi^2\sigma^*$ configuration, the last three of which, $3\ ^3\Sigma^-$, $2\ ^1\Delta$, and $2\ ^1\Sigma^+$, not yet considered here, lie significantly higher in energy and strongly interact with Rydberg states. This range of excitation energies, from 50 000 to 75 000 cm^{-1}, is enlarged in Fig. 2 to give a better idea of the low-lying Rydberg states of AsH. The lowest pair of them, $3\ ^{3,1}\Pi$, arises from the $\sigma^2\pi\sigma_R$ configuration, but there are some other electronic configurations such as $\sigma\pi^2\sigma_R$, $\sigma^2\pi\pi_R$, or $\sigma^2\pi\sigma_R^*$ which produce numerous Rydberg states of various symmetries in this energy range. As expected, all of them are characterized by deep minima and equilibrium distances which are approximately equal to that of the $X\ ^3\Sigma^-$ ground state, but there are many avoided crossings with the repulsive valence states producing a complicated appearance for the potential diagram in this range.

IV. POTENTIAL-ENERGY RESULTS WITH SPIN–ORBIT COUPLING

After the introduction of spin–orbit coupling the $\Lambda-S$ states discussed above split into various components with a definite Ω quantum number. Potential-energy curves for the valence Ω states are shown in Fig. 3, and for each of the Ω values from 0^+ to 2 separately in Figs. 4–7, in which the Rydberg states are also included. The present computed spectroscopic constants for the low-lying states are given in Table III, together with available experimental and previous theoretical values for these quantities. Though being very important for describing radiative and predissociation processes, the spin–orbit interaction does not greatly affect the shapes of the AsH potential curves in most cases. Therefore

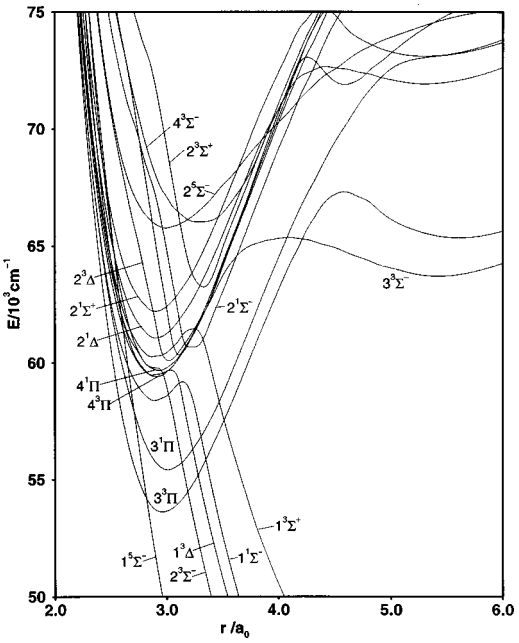

FIG. 2. Computed potential-energy curves of the lowest Rydberg $\Lambda-S$ states of AsH obtained without inclusion of the spin–orbit interaction.

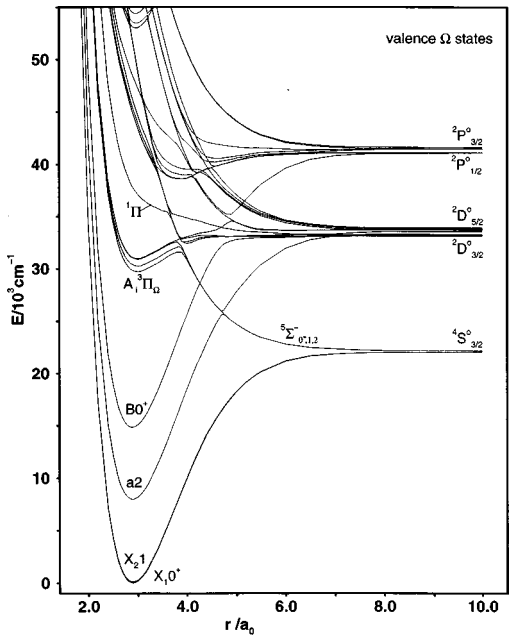

FIG. 3. Computed potential-energy curves of the valence Ω states of AsH obtained after inclusion of the spin–orbit interaction.

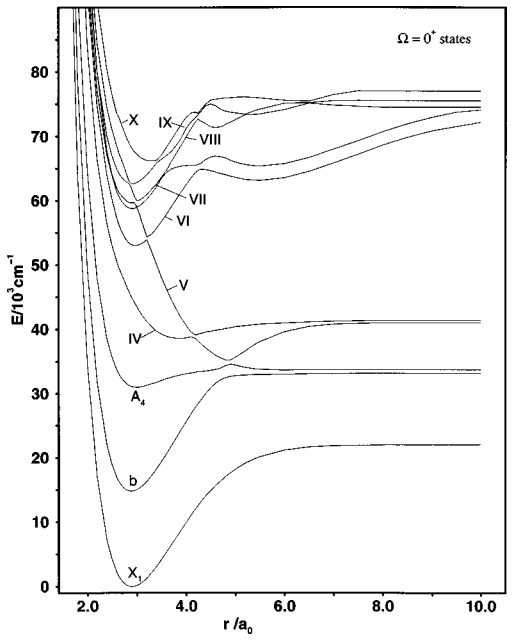

FIG. 4. Computed potential-energy curves for the ten lowest $\Omega=0^+$ states of the AsH radical.

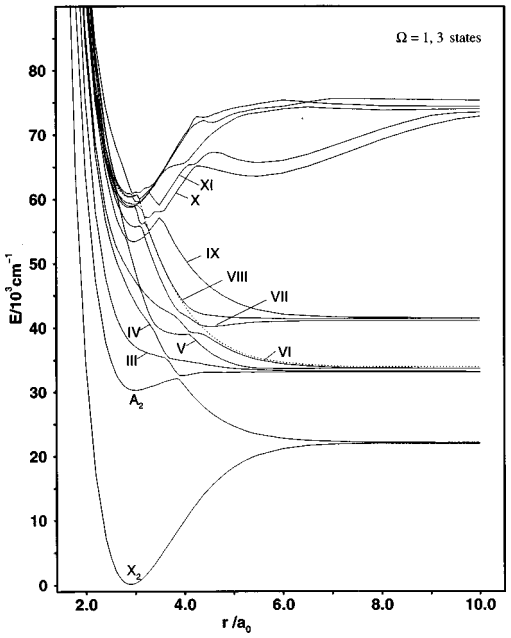

FIG. 6. Computed potential-energy curves for the fourteen lowest $\Omega=1$ states of the AsH radical. The dashed curve corresponds to the lowest $\Omega=3$ state of the system.

we shall often use the $\Lambda-S$ notation in the following narration to underline the origin of the states to be discussed.

The $X\ ^3\Sigma^-$ ground state is split into 0^+ and 1 components. This splitting is calculated to be 107 cm^{-1} and, as was correctly noted earlier,[3,10] is mainly caused by the spin–orbit interaction with the $b\ ^1\Sigma^+$ state, which lowers the energy of the 0^+ component of the ground state by 108.6 cm^{-1}. Spin–orbit interaction of $X\ ^3\Sigma^-$ with other $^{1,3}\Sigma^+$ and $^{1,3}\Pi$ states is not negligible, but it decreases fairly quickly with excitation energy of the perturbing state. For example, the contribution to the $X_1 0^+$ shift from the $1\ ^3\Pi$ state is 13.29 cm^{-1}, whereas from the $7\ ^3\Pi$ and $8\ ^3\Pi$ together, it is only 0.013 cm^{-1}. It also follows from the present calculations (the same as found in Ref. 10) that interaction with the higher-lying states leads to approximately the same shift for the 0^+ and 1 ground state components, so that the final result for the $X\ ^3\Sigma^-$ splitting changes by less than 2 cm^{-1}. As one can see from Table III, the computed $X\ ^3\Sigma^-$ zero-field splitting is slightly smaller

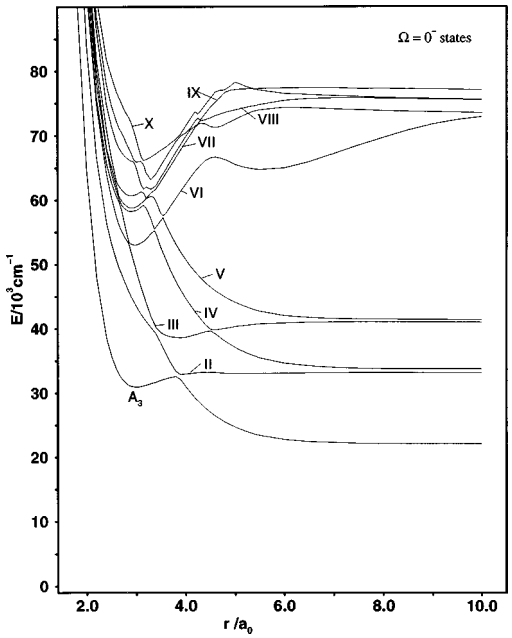

FIG. 5. Computed potential-energy curves for the ten lowest $\Omega=0^-$ states of the AsH radical.

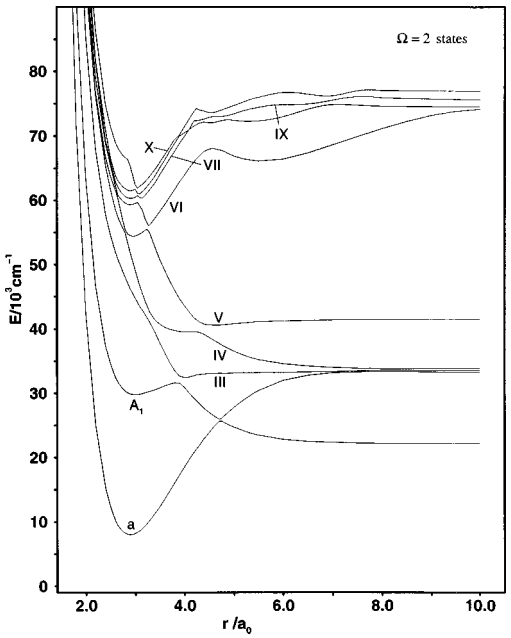

FIG. 7. Computed potential-energy curves for the ten lowest $\Omega=2$ states of the AsH radical.

TABLE III. Calculated and experimental spectroscopic constants of AsH (transition energies T_e, bond lengths r_e, and vibrational frequencies ω_e).

	T_e/cm^{-1}		r_e/Å		ω_e/cm^{-1}	
State	Calc.	Expt.	Calc.	Expt.	Calc.	Expt.
$X_1\ ^3\Sigma^-_{0^+}$	0	0	1.535	1.5232 [1]	2163	2183 [4]
			1.523 [9]	1.523 15 [5]	2151 [9]	2175 [5]
			1.5335 [10]	1.5231 [6]	2373 [10]	2155 [6]
			1.528 [12]		2194 [12]	
$X_2\ ^3\Sigma^-_1$	107	117.6 [6]	1.535		2163	
	101 [10]					
$a\ ^1\Delta_2$	7774	7217 [1]	1.532	1.5203 [1]	2202	2180 [1]
	8709 [10]		1.532 [10]		2134 [10]	
	9968 [12]		1.525 [12]		2190 [12]	
$b\ ^1\Sigma^+$	14 621	14 178 [7]	1.528	1.529 37 [7]	2228	2213 [7]
	15 295 [10]		1.526 [10]		2176 [10]	
	17 114 [12]		1.522 [12]		2197 [12]	
$A_1\ ^3\Pi_2$	29 750	29 282[a] [3]	1.598	1.581[b] [3]	1533	(1207.5)[c] [3]
$A_2\ ^3\Pi_1$	30 287	29 822[a] [3]	1.599	1.582[b] [3]	1524	
$A_3\ ^3\Pi_{0^-}$	30 945		1.598	1.580[b] [3]	1526	
$A_4\ ^3\Pi_{0^+}$	30 985	30 518[a] [3]	1.596	1.578[b] [3]	1539	
$3\ ^3\Pi_{0^+}$	52 963		1.578		2558	

[a] ν_{00} value.
[b] r_e values determined in Ref. 3 for AsD.
[c] $\Delta G(1/2)$ value.

than the experimental result. In our opinion, there are two reasons for such an underestimation. First of all, as we have seen from the As atomic tests (Table I), there is a small underestimation of the $^2D°$ and $^2P°$ SO splittings, and one can assume that this is characteristic of the spin-dependent part of the RECP employed. Secondly, one can see from Table III that the excitation energy of the $b\ ^1\Sigma^+$ state is overestimated in the present study by 443 cm^{-1} and this alone leads to an underestimation of the $X\ ^3\Sigma^-$ splitting of $\approx$3.5 cm^{-1}. In other words, there are two fairly small effects which add to produce the final discrepancy of $\approx$11 cm^{-1} relative to the experimental value.

The r_e value computed in this work for the X_1 component is 1.535 Å, which agrees well with the previous calculated and experimental results. It is slightly larger (by 0.012 Å) than the experimentally determined value of 1.523 Å, and since perfect agreement with the experimental result has been obtained in the only calculation[9] in which the $3d$ electrons were included in the correlation treatment, one can conclude that the slight overestimation found in the present work as well as in Refs. 10 and 12 is caused by the absence of the $3d$ electron correlation in these studies. The calculated ω_e value of 2163 cm^{-1} also agrees very well with the experimental data, which fall in the range of 2155–2183 cm^{-1} (see Table III). The r_e and ω_e values of both X_1 and X_2 components are found to be the same at the present level of accuracy, indicating that the SO interaction effect on these quantities is very small. The dissociation energy D_e of the ground $X_1\ ^3\Sigma^-_{0^+}$ state has been estimated in the present study as the average of all five Ω roots (two for $X\ ^3\Sigma^-$ and three for $^5\Sigma^-$) going to the lowest As($^4S°$)+H(^2S) dissociation limit. The resulting D_e value is 22 213 cm^{-1} (2.75 eV), which agrees well with the experimentally determined D_0 $=22\ 300\pm1000$ cm^{-1} (2.76 eV),[3] 2.80 ± 0.03 eV[8] as well as with the earlier calculated results: $D_e=2.82$,[9] 2.83,[10] and 2.71 eV.[11]

The first excited state of AsH is $a\ ^1\Delta$. Its excitation energy is calculated to be 7774 cm^{-1}, 557 cm^{-1} higher than the experimental result. Such an overestimation is anticipated on the basis of the As atomic tests (Sec. II) and the well-known problem of correlating singlet states at the same level of accuracy as triplets. This discrepancy is significantly smaller than in the previous calculations,[10,12] however, which give overestimations of the T_e value by $\approx$1500 and 2750 cm^{-1}, respectively. The computed r_e value for the $a\ ^1\Delta$ state is 0.003 Å smaller than that for the X state, exactly the same margin as found experimentally, indicating that the relative accuracy of the present calculations is noticeably better than the absolute. Shortening of the $a\ ^1\Delta$ state equilibrium distance with respect to that of the ground state has also been found in the other theoretical studies[10,12] and can be qualitatively explained by the fact that the $a\ ^1\Delta$ state converges adiabatically to the As($^2D°$) limit, which lies 10 592 cm^{-1} higher than $^4S°$ and thus should have a steeper attractive limb for its potential curve than X_1. This also explains the somewhat higher vibrational frequency determined for this state, both theoretically and experimentally, as compared to the X_1 ω_e value. On its way to the dissociation limit the $a\ ^1\Delta$ state undergoes an avoided crossing with the repulsive $^5\Sigma^-$ state, but this crossing is very sharp due to the weakness of the SO interaction between states with $\Delta\Lambda=2$.

The excitation energy to the next $b\ ^1\Sigma^+$ state is calculated to be 14 621 cm^{-1}, once again noticeably lower than in the previous theoretical studies,[10,12] and thus in much better

agreement with the measured value of 14 178 cm^{-1}. The computed r_e value for this state agrees perfectly with the only available experimental result.[7] This is a surprising result, however, since for the same reasons as for the $a\ ^1\Delta$ state, $b\ ^1\Sigma^+$ should have a shorter bond distance than X_1. Moreover, the direct spin–orbit interaction between $b\ ^1\Sigma^+$ and $X_1\ ^3\Sigma^-_{0^+}$, which increases with distance, should lead to a further shortening. Careful analysis of Ref. 7 shows that the equilibrium distance value determined for the $b\ ^1\Sigma^+$ state should be considered as r_0 rather than r_e (though the r_e designation has been used), since it is based on the B_0 rotational constant determined in the latter study. One can also assume, based on the r_e experimental value for the ground state and corresponding results of the present calculations, that the correct r_e value for the $b\ ^1\Sigma^+$ state should lie in the 1.516–1.520 Å range. The calculated ω_e value is 2228 cm^{-1}, in very good agreement with the observed result of 2213 cm^{-1}.[7]

The $A\ ^3\Pi$ multiplet, lying next in energy, is the first state of AsH to show a truly strong effect of the spin–orbit interaction. Its $\Omega=2$ component is computed to lie at 29 750 cm^{-1}, slightly higher than measured in the absorption spectrum.[3] Employing the calculated T_e and ω_e values for the $X_1\ ^3\Sigma^-_{0^+}$ and $A_1\ ^3\Pi_2$ states from Table III, one obtains $\nu_{00}=29\,435\ cm^{-1}$, in good agreement with the measured value of 29 282 cm^{-1}.[3] The $^3\Pi_1-^3\Pi_2$ SO splitting is calculated to be 537 cm^{-1}, in excellent agreement with the measured value of 540 cm^{-1}. The $^3\Pi_{0^+}$ state lies 698 cm^{-1} higher than $^3\Pi_1$, which also agrees very well with the 696 cm^{-1} result determined in Ref. 3. The second-order 0^+-0^- splitting is calculated to be 40 cm^{-1}, as compared to the experimental value of 44.7 cm^{-1}. It is worthwhile to note at this place that though such (almost perfect) agreement of the computed and measured SO splittings for the $A\ ^3\Pi$ multiplet is probably fortuitous, the overall agreement of the spin–orbit effects on the low-energy electronic structure of AsH obtained in the present study with the available spectroscopic data is very good and consistent. This allows one to conclude that the full-core RECP for the As atom from Ref. 16 provides a reliable description of such effects, with perhaps some tendency toward slight underestimation. This view is also supported by direct comparison of SO matrix elements for the low-lying $\Lambda-S$ states computed in the present work and in the all-electron calculation[10] in the case when scalar relativistic effects have been included in the latter study. For example, the $\langle X\ ^3\Sigma^-|H_{\mathrm{SO}}|b\ ^1\Sigma^+\rangle$ and $\langle A\ ^3\Pi_x|H_{\mathrm{SO}}|A\ ^3\Pi_y\rangle$ matrix elements are calculated in the present study to be 1254 and 600 cm^{-1}, respectively, in good agreement with the values of 1242 and 596 cm^{-1} obtained in Ref. 10. It was found in Ref. 10 that the corrected description of the orbital expansions due to scalar relativistic effects is important for obtaining appropriate spin–orbit splittings and the above comparison shows that the present RECP allows one to achieve this goal as well.

The calculated r_e values for the various Ω components differ very little and are 0.017–0.018 Å larger than the measured ones, such an overestimation being typical for the present study. Differences among the calculated frequencies are also quite small ($\leqslant 15\ cm^{-1}$), but unfortunately it is difficult to compare them with experimental data since only a $\Delta G(1/2)$ value for the 0^+ component is available. It has been correctly argued in Ref. 3 that the reason why the $v'=1$ vibrational level has been observed only for the $A\ ^3\Pi_{0^+}$ state, is predissociation of the $A\ ^3\Pi$ multiplet by the repulsive $^5\Sigma^-$ state, and this explanation can be put on more quantitative grounds on the basis of the present results. One can see from Figs. 3 and 5–7 that strong spin–orbit interaction between the $\Omega=2$, 1, and 0^- components of the $A\ ^3\Pi$ and $^5\Sigma^-$ multiplets leads to distinct maxima on the former potential curves. The corresponding well depths are about 1800–2000 cm^{-1}, which thus are not able to contain more than one vibrational level. The only exception is the $A\ ^3\Pi_{0^+}$ state, which does not interact with the $^5\Sigma^-$ because of symmetry. This state has a very peculiar right limb, however, due to the strong spin–orbit interaction of $A_4\ ^3\Pi_{0^+}$, $b\ ^1\Sigma^+$, and $2\ ^3\Sigma^-$ in the 4.8–5.0 a_0 range of internuclear distance (see Figs. 3 and 4). So it is inconsistent to compare the ω_e value calculated in the present study as a second derivative at the equilibrium distance with the observed energy difference between the $v'=1$ and 0 levels. Using approximate Morse curves, Dixon and Lamberton[3] have estimated the $b\ ^1\Sigma^+-A_4\ ^3\Pi_{0^+}$ crossing to occur at $r\approx 2.6$ Å$(4.9\ a_0)$, which agrees very well with the present finding, with the only correction that three states, b, A_4, and $2\ ^3\Sigma^-$, rather than two, strongly interact in this distance range.

It has also been noted in the experimental study[3] that observed lines in $A\ ^3\Pi-X\ ^3\Sigma^-$ absorption are sharp for the $^3\Pi_{0^+}$ substrate and increase in width in the order $^3\Pi_{0^+}<{}^3\Pi_{0^-}<{}^3\Pi_1<{}^3\Pi_2$. It has been concluded in Ref. 3 that the reason for such behavior is the strength of the $A\ ^3\Pi-{}^5\Sigma^-$ SO interaction, which according to the Wigner–Eckart theorem should increase in the same sequence. The present accurate calculation of this effect confirms this conclusion, which can be seen from the increasingly larger energy splittings for states with $\Omega=0^-$, 1, and 2, respectively. The $A_4\ ^3\Pi_{0^+}$ state is twice as deep ($\approx 3600\ cm^{-1}$) as the other Ω components, but higher rotational levels of the $v'=1$ level may be already predissociated due to nonzero probability of tunneling through the relatively narrow barrier at its attractive limb. The possibilities for spectroscopic observation of the $A\ ^3\Pi-X\ ^3\Sigma^-$ transitions become more favorable in AsD due to a noticeably smaller vibrational quantum in this case. Thus it is not surprising that transitions to the $v'=1$ levels have been observed for all $A\ ^3\Pi$ substates of AsD.[3]

Having employed relationships between spectroscopic constants for Morse potentials, the authors of Ref. 3 concluded that the $^3\Pi_0$, $^3\Pi_1$, and $^3\Pi_2$ states should go to the same dissociation limit of $32\,900\pm 1000\ cm^{-1}$. As the present calculations show (Fig. 3), the 0^-, 1, and 2 components really do go to the same $\mathrm{As}(^2D_{3/2})+\mathrm{H}(^2S_{1/2})$ atomic asymptote, which is estimated in the present study for the internuclear separation of 10.0 a_0 to lie at 33 274 cm^{-1}, in good agreement with the above experimental result. The $A_4 0^+$ state (the third 0^+ root) goes to the $\mathrm{As}(^2D_{5/2})$

$+\mathrm{H}(^2S_{1/2})$ limit, however, which is calculated to lie $\sim 500\ \mathrm{cm}^{-1}$ higher at $r=10.0\ a_0$, while the second 0^+ root, which is mainly $^1\Sigma^+$ in the Franck–Condon region, takes on predominantly $^3\Pi$ character at longer distances and converges to the $\mathrm{As}(^2D_{3/2})+\mathrm{H}(^2S_{1/2})$ asymptote.

The energy range from 32 000 to 42 000 cm^{-1} is characterized by a high density of states, a number of which, e.g., 0^+(IV,V), 0^-(III), 1(III, VII) etc. (Figs. 4–7), have potential minima. It will probably be difficult to observe these states spectroscopically, however, due to numerous avoided and allowed crossings which occur in this region and cause predissociation of the above states. As has already been mentioned in the discussion of the $\Lambda-S$ level calculations (Sec. III), the $^1\Pi$ state is repulsive and this feature is not changed upon inclusion of the SO interaction. This finding contradicts the results of a previous calculation[12] and indicates that the $^1\Pi$ state cannot serve as a suitable candidate for the laser excitation experimental scheme discussed in Sec. I.

There is a gap in the AsH electronic spectrum from 42 000 to 53 000 cm^{-1}, at which energy the first Rydberg state appears, $3\ ^3\Pi(\sigma^2\pi\sigma_R)$. As one can see from Figs. 3–7, this state is strongly bound and split by the SO interaction into Ω components with regular ordering. The calculated spectroscopic constants for the lowest 0^+ component of $3\ ^3\Pi$ (almost degenerate with 0^-) are given in Table III, and the corresponding 1 and 2 components lie higher by 460 and 1370 cm^{-1}, respectively. It appears that it should be possible to observe the $3\ ^3\Pi$ substates spectroscopically, especially in absorption, but there may be difficulties since all of them are predissociated due to avoided crossings with the repulsive limbs of valence state potential curves which converge to much lower-lying atomic asymptotes. Some other Rydberg states also are shown in Figs. 4–7, but the electronic structure becomes very complicated in this energy range and will not be discussed further.

V. DIPOLE MOMENTS, TRANSITION MOMENTS, AND RADIATIVE LIFETIMES

A. Electric dipole moments

Electric dipole moments μ have been computed for a number of low-lying electronic states of AsH as a function of internuclear distance and these data are presented in Fig. 8. One can see from this figure that the dipole moments of the lowest three electronic states, $X\ ^3\Sigma^-$, $a\ ^1\Delta$, and $b\ ^1\Sigma^+$ have almost a linear dependence on the internuclear distance and differ very little in the whole range of distances considered. This shows that the distribution of electronic density in all these states is mainly defined by their common $\sigma^2\pi^2$ electronic configuration. This is especially true near their approximate equilibrium distances ($r_e=2.9\ a_0$), where $\sigma^2\pi^2$ plays a dominant role, but somewhat larger differences appear at longer and shorter nuclear separations, for which contributions from other electronic configurations become nonnegligible. The dipole moments of all above states have small positive values at r_e, which corresponds to $\mathrm{As}^-\mathrm{H}^+$ polarity, indicating that the electronic density in the bonding σ MO is slightly shifted towards the As atom. At larger bond

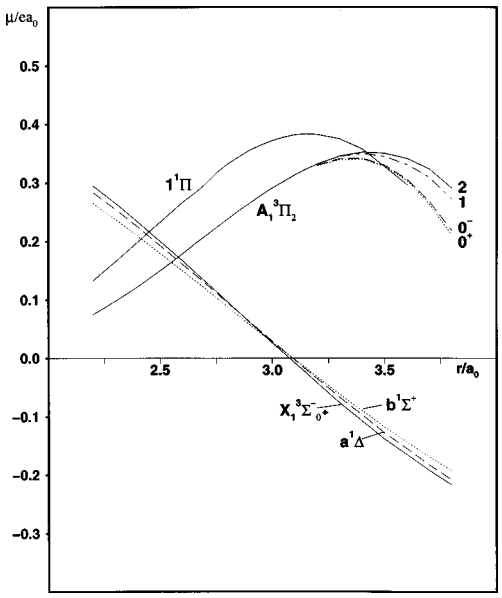

FIG. 8. Computed electric dipole moments for a number of low-lying states of the AsH radical. Results for the $A\ ^3\Pi\ \Omega=0^+$, 0^-, and 1 components are given only for $r\geqslant 3.4\ a_0$. A positive value indicates a positive charge on the hydrogen atom.

distances ($r\geqslant 3.1\ a_0$), however, the dipole moments change their signs due to stronger contributions of the $1s$ hydrogen AO to the σ MO of AsH. The difference between the calculated dipole moments of the X_1 and X_2 ground state Ω components is always smaller than $1.3\cdot 10^{-3}\ ea_0$, which shows that the influence of the SO interaction on this quantity is very weak. For this reason only the X_1 dipole moment curve is given in the figure.

As one can see from Fig. 8, the next most stable excited states, $A\ ^3\Pi$ and $1\ ^1\Pi$, also have positive dipole moment values in the Franck–Condon region, but they are considerably larger than for the lowest states discussed first. This is easily understandable since both Π states stem from the $\sigma\pi^3$ configuration, with the π MO being much more strongly localized on the As atom than σ. The influence of the SO interaction on the dipole moment curves of the $A\ ^3\Pi$ components is small, so that they almost coincide up to an internuclear distance of $3.4\ a_0$. Beyond this the SO interaction with other states, above all with $^5\Sigma^-$, produces larger differences in the μ values, which are then given as separate curves for $\Omega=2,1$, 0^+, and 0^-. It is also interesting to note that the next pair of $^{1,3}\Pi$ states has negative dipole moment values (e.g., $\mu=-0.102\ 27\ ea_0$ for $2\ ^3\Pi_{0+}$ at $2.9\ a_0$) and this is caused by the fact that they arise from the $\sigma^2\pi\sigma^*$ configuration, with the σ^* MO localized more strongly on the hydrogen atom.

Dipole moment curves for the $^3\Sigma^-$, $^1\Delta$, and $^{1,3}\Pi$ states of AsH have also been calculated in Ref. 12 (without including SO coupling) and the overall agreement with the present results in the $2.2-3.8\ a_0$ distance range is good, with a trend toward somewhat smaller μ values in the present study. For example, for the $X\ ^3\Sigma^-$ state $\mu=0.178$ D (0.156 D) has been calculated[12] at r_e, and for $^1\Delta$ and $^1\Pi$ $\mu=0.205$ D

TABLE IV. Calculated electric dipole moment values (in ea_0) for the low-lying electronic states ($v=0$) of AsH and BiH (Ref. 13). A positive value indicates a positive charge on the hydrogen atom.

AsH		BiH	
State	μ	State	μ
$X_1\ ^3\Sigma^-_{0^+}$	0.0498	$X_1 0^+$	−0.3760
$X_2\ ^3\Sigma^-_1$	0.0501	$X_2 1$	−0.2710
$a\ ^1\Delta$	0.0531	$a2$	−0.2252
$b\ ^1\Sigma^+$	0.0522	$B0^+$	−0.1269
$A_4\ ^3\Pi_{0^+}$	0.2997	$E0^+$	−0.7924

(0.159 D), 0.779 D (0.674 D), respectively, where values of the present calculation are given in parentheses. A larger value of the dipole moment of the ground state has also been obtained in Ref. 9, in which no relativistic effects have been included. Such effects, especially the scalar part of them, usually lead to a contraction of electron density which should result in smaller μ values, consistent with the present calculations. The authors of Ref. 9 have also noted that their computed AsH dipole moment would agree better with the linear relationship between dipole moments and electronegativities of the third-row main group hydrides if a slightly larger value (2.1–2.2) were used for the As atom electronegativity (see Fig. 1 of Ref. 9). On the other hand, the same relationship could be satisfied if the AsH μ value were slightly smaller (0.10–0.15 D) than computed in Ref. 9, which is consistent with the present findings. The present study is also not free from deficiencies (e.g., no explicit treatment of the As $3d$ electrons), however, so that only experiment can give a final answer to this question.

Dipole moment values calculated for the lowest ($v=0$) vibrational level of a number of AsH electronic states are given in Table IV in comparison with the earlier results obtained for the corresponding states of BiH.[13] One can see from this table that, unlike the situation in AsH, all BiH low-lying states are characterized by negative dipole moment values, which is a direct consequence of the much lower electronegativity of the Bi atom relative to As. The dipole moment of the $X_2 1$ state of BiH is 0.105 ea_0 smaller in magnitude than that of the $X_1 0^+$ state, indicating that the effects of spin–orbit coupling are far from being negligible in this system, once again unlike the situation in AsH. One can also note that the analogy between the AsH and corresponding BiH states is only quite straightforward for the lowest three states, since very strong SO coupling in the latter system leads to significant changes in the $\Lambda-S$ character of the $B0^+$ and $E0^+$ states from almost pure $^1\Sigma^+$ and $^3\Pi$ in AsH to a complicated mixture of $^3\Sigma^+$, $^1\Sigma^+$, $1\ ^3\Pi(\sigma\pi^3)$, and $2^3\Pi(\sigma^2\pi\sigma^*)$ states in BiH.[13]

B. Transition moments and radiative lifetimes

Electric dipole transition moments for radiative transitions between the four lowest $\Lambda-S$ states of AsH are given as a function of internuclear distance in Table V. These results are also averaged for various combinations of vibrational functions and the radiative lifetimes computed on this basis are summarized in Table VI.

The X_2-X_1 transition moment is calculated to be very small ($0.69\cdot10^{-4}\ ea_0$), as can be expected for a transition between two spin components of the $^3\Sigma^-$ state, which is relatively weakly influenced by the spin–orbit interaction. Combined with the X_2-X_1 spin–orbit splitting of 117.6 cm^{-1} this gives an extremely small transition probability of $1.6\cdot10^{-6}$ s^{-1} computed as an estimate at $r=2.9\ a_0$. We suppose, however, that other effects not considered in the present study, such as magnetic dipole transitions and nonadiabatic interactions (e.g., spin–rotation coupling) may be important for obtaining the final transition probability and radiative lifetime values for this transition.

The first excited state, $a\ ^1\Delta$, has an allowed electric-dipole transition to the upper $X_2\ ^3\Sigma^-_1$ ground-state component, but it is also quite weak, being doubly forbidden at the $\Lambda-S$ level due to the different multiplicity and $\Delta\Lambda=2$ for the states involved. As was correctly noted in Ref. 10, this transition mainly borrows its intensity from the $^3\Pi-X\ ^3\Sigma^-$ and $a\ ^1\Delta-{}^1\Pi$ $\Lambda-S$ transitions. The $A\ ^3\Pi-X\ ^3\Sigma^-$ and $a\ ^1\Delta-1\ ^1\Pi$ contributions are the two largest, but they partly cancel each other, and therefore it is also necessary to include the higher-lying $^3\Pi$ and $^1\Pi$ states into the $\mu(a-X_2)$ computation. Eight roots for each $^1\Pi$ and $^3\Pi$ symmetry have been included in the present calculation and, though contributions from the higher-lying Rydberg states are noticeably smaller than those of the valence states, it has been found that they are far from being negligible. The computed radiative lifetime of the $a\ ^1\Delta(v=0)$ state is 97 ms, significantly longer than the 22 ms value estimated in Ref. 10 at the r_e distance. There are two reasons for this difference. First of all, the $a-X_2$ transition moment calculated in Ref. 10 is somewhat larger, $5.775\cdot10^{-3}$ versus $3.48\cdot10^{-3}\ ea_0$ obtained in the present study. Secondly, the excitation energy of the $a\ ^1\Delta$ state is 935 cm^{-1} higher than in the present work, and this gives a noticeably higher ν^3 frequency factor for the $a-X_2$ Einstein coefficients. The transition moment dependence on the internuclear distance is not negligible, giving a τ value, obtained upon averaging over vibrational wave functions, which is 7 ms larger than the corresponding estimate at r_e, but this difference does not play a decisive role. The $a-X_1$ transition, which is possible due to a quadrupole term, has been calculated earlier[10] to have a very long radiative lifetime of $2.2\cdot10^3$ s, so that the $a-X_2$ transition is without doubt the main channel of the $a\ ^1\Delta$ state radiative decay. Although the $a-X_2$ transition has already been observed, no experimental τ value is available for comparison with the calculated data.

The $b\ ^1\Sigma^+$ state, which is next in energy, has two dipole-allowed transitions to the lower-lying states, namely to the $X_1 0^+$ and $X_2 1$ components of the ground state. One can see from Tables V and VI that the perpendicular $b-X_2$ transition is much stronger than the parallel $b-X_1$. This situation is opposite to that in BiH,[13] and this difference can be understood on the basis of the electron density distribution in both systems (see also Refs. 13, 14, and 28). The parallel

transition moment is to a first approximation proportional to the difference of the dipole moments of the b and X_1 states. This difference is very small (0.0042 ea_0 at $r_e=2.9$ a_0) for the AsH radical (see Sec. V A) and relatively large (0.249 ea_0) for BiH, which leads to a shorter partial radiative lifetime (5.2 μs) by more than three orders of magnitude for the $b-X_1$ transition in the latter system. The perpendicular $b-X_2$ transition borrows its intensity mainly from the $^3\Pi-X\ ^3\Sigma^-$ and $b\ ^1\Sigma^+-{}^1\Pi$ transitions which come into play due to admixture of the $^3\Pi$ and $^1\Pi$ character to the $b\ ^1\Sigma^+$ and $X\ ^3\Sigma^-$ states, respectively. The spin–orbit interaction which is responsible for this effect is significantly stronger in BiH than in AsH and therefore the corresponding radiative lifetime is noticeably shorter in this case: 24.4 μs (BiH) vs 950 μs (AsH). This change is not so dramatic as for the $b-X_1$ transition, however, and hence the transition to the X_2 state is the dominant channel of the $b\ ^1\Sigma^+$ state radiative decay in the AsH radical. The $b-X_1$ partial lifetime value, computed in the present study to be 44 ms, agrees quite well with the τ value of 35 ms determined in Ref. 10. For the $b-X_2$ transition we obtain 950 μs, which is almost three times longer than the 350 μs value calculated in Ref. 10. This discrepancy, similar to the case of the $a-X_2$ transition discussed above is caused by the overestimation of the b state excitation energy as well as by a somewhat larger transition moment computed in Ref. 10. An experimental esti-

TABLE V. Computed transition dipole moments μ (in ea_0) between $X_1\ ^3\Sigma^-_{0^+}$, $X_2\ ^3\Sigma^-_1$, $a\ ^1\Delta$, $b\ ^1\Sigma^+$, and $A_i\ ^3\Pi_\Omega$ states of the AsH radical at various bond lengths r (in a_0).

	μ						
r	$a-X_2$	$B-X_1$	$B-X_2$	A_1-X_2	A_1-a	A_2-X_1	A_2-X_2
2.30	0.005 91	0.001 16	−0.015 83	0.215 90	−0.006 82	0.303 52	−0.003 95
2.40	0.005 62	0.001 15	−0.014 63	0.205 87	−0.004 64	0.289 92	−0.002 65
2.50	0.005 29	0.001 13	−0.013 22	0.195 52	−0.002 38	0.275 66	−0.001 26
2.60	0.004 60	⋯	−0.012 16	0.184 97	−0.000 05	0.260 53	0.000 22
2.66	⋯	0.001 15	⋯	0.178 42	0.001 39	0.251 93	0.001 20
2.70	0.004 27	0.001 19	−0.011 46	0.173 11	0.002 36	0.244 88	0.001 85
2.75	⋯	0.001.26	⋯	0.167 66	0.003 59	0.236 30	0.002 70
2.80	0.003 91	0.001 33	−0.010 73	0.161 41	0.004 84	0.227 33	0.003 60
2.86	0.003 66	0.001 40	−0.009 88	0.153 87	0.006 36	0.216 74	0.004 75
2.90	0.003 48	0.001 49	−0.009 28	0.147 97	0.007 39	0.209 47	0.005 57
2.95	0.003 20	0.001 58	−0.008 58	0.142 29	0.008 71	0.200 27	0.006 61
3.00	0.002 97	⋯	−0.008 02	0.135 94	0.010 05	0.190 74	0.007 75
3.05	0.002 73	0.002 32	−0.007 51	0.129 46	0.011 41	0.181 11	0.009 06
3.10	0.002 54	0.002 65	−0.007 04	0.122 57	0.012 87	0.171 30	0.010 38
3.15	⋯	0.003 01	⋯	0.115 47	0.014 33	0.161 04	0.011 66
3.20	0.002 31	0.003 23	−0.006 33	0.108 63	0.015 86	0.151 20	0.013 14
3.30	0.001 78	0.003 75	−0.005 58	0.094 49	0.018 99	0.131 31	0.015 31
3.40	0.001 66	0.004 36	−0.004 72	0.080 75	0.022 35	0.110 51	0.017 61
3.50	0.001 46	0.004 90	−0.003 79	0.066 44	0.025 60	0.089 76	0.019 73
3.60	0.001 36	0.005 77	−0.003 00	0.052 69	0.028 96	0.068 92	0.021 93
3.70	0.001 27	0.006 60	−0.002 13	0.039 88	0.032 20	0.049 67	0.024 02

r	A_2-a	A_2-b	A_3-X_2	A_4-X_1	A_4-X_2	A_4-b
2.30	0.018 37	0.011 25	0.216 16	−0.004 98	0.212 77	−0.006 08
2.40	0.017 86	0.010 66	0.205 42	−0.003 39	0.203 66	−0.003 89
2.50	0.017 25	0.009 96	0.194 78	−0.001 72	0.193 92	−0.001 52
2.60	0.016 60	0.009 34	0.184 14	0.000 07	0.183 17	0.000 92
2.66	0.016 27	0.008 94	0.177 52	0.001 29	0.177 61	0.002 41
2.70	0.016 16	0.008 53	0.172 11	0.002 08	0.172 96	0.003 37
2.75	0.016 00	0.007 70	0.166 59	0.003 10	0.166 30	0.004 64
2.80	0.015 69	0.006 48	0.160 27	0.004 19	0.159 70	0.005 82
2.86	0.015 35	0.005 84	0.152 61	0.005 62	0.152 28	0.007 28
2.90	0.015 25	0.005 47	0.146 44	0.006 62	0.147 94	0.008 18
2.95	0.015 07	0.005 01	0.140 67	0.007 92	0.140 61	0.009 37
3.00	0.014 93	0.004 57	0.134 10	0.009 36	0.133 49	0.010 74
3.05	⋯	0.004 04	0.127 29	⋯	0.126 49	0.014 28
3.10	⋯	⋯	0.119 97	0.012 36	0.199 49	0.015 56
3.15	⋯	⋯	0.112 49	⋯	0.112 09	0.016 93
3.20	0.014 15	0.001 90	0.105 12	0.015 73	0.104 75	0.019 52
3.30	0.013 69	0.001 10	0.090 49	0.018 50	0.090 47	0.022 07
3.40	0.012 88	0.000 24	0.074 91	0.021 53	0.074 39	0.024 57
3.50	0.011 93	−0.000 69	0.059 15	0.024 27	0.058 41	0.026 84
3.60	0.010 89	−0.001 48	0.042 81	0.027 20	0.042 09	0.028 93
3.70	0.009 66	−0.002 17	0.027 29	0.030 05	0.026 71	0.030 74

TABLE VI. Calculated radiative lifetimes (in s) of excited states ($v'=0$) of AsH: Partial lifetimes τ_p for transitions to $X_1\ ^3\Sigma_{0^+}^-$, $X_2\ ^3\Sigma_1^-$, $a\ ^1\Delta$, and $b\ ^1\Sigma^+$, respectively, and total lifetime τ.[a]

State	$\tau_p(X_1)$	$\tau_p(X_2)$	$\tau_p(a)$	$\tau_p(b)$	τ
$a\ ^1\Delta$	⋯	97(−3)	⋯	⋯	97(−3)
$b\ ^1\Sigma^+$	44(−3)	0.95(−3)	⋯	⋯	0.93(−3)
$A_1\ ^3\Pi_2$	⋯	1.26(−6)	298(−6)	⋯	1.25(−6)
$A_2\ ^3\Pi_1$	0.61(−6)	164(−6)	228(−6)	8.5(−3)	0.61(−6)
$A_3\ ^3\Pi_{0^-}$	⋯	0.59(−6)	⋯	⋯	0.59(−6)
$A_4\ ^3\Pi_{0^+}$	105(−6)	0.58(−6)	⋯	598(−6)	0.58(−6)

[a]Values in parentheses denote powers of ten.

mate of the total radiative lifetime of the $b\ ^1\Sigma^+$ state made recently on the basis of the observed emission from this state is $\geqslant 800\ \mu$s[29] and favors the longer lifetime value obtained in the present study.

The $A\ ^3\Pi$ multiplet is the first excited state to have a $\Lambda-S$ allowed transition to the ground state. There are four possible Ω combinations for the $^3\Pi-^3\Sigma^-$ perpendicular transition and they have similar partial lifetimes of 0.6–1.3 μs. Spin–orbit interaction also makes parallel $A\ ^3\Pi-X\ ^3\Sigma^-$ transitions allowed, but as can be seen from Tables V and VI, they are much weaker than those of perpendicular type. This is a clear indication of the relative weakness of the SO interaction in AsH compared with the heavier BiH radical, for which the SO interaction is so strong that it practically eliminates any distinction between spin-allowed and forbidden transitions.[13] The $A_1\ ^3\Pi_2$ and $A_2\ ^3\Pi_1$ states also have fairly strong transitions to the $a\ ^1\Delta$ state and this means that they are good candidates for the (laser induced fluorescence) LIF experimental scheme discussed in the Introduction. There should be no problems in exciting these states from the $a\ ^1\Delta$ state and they will decay mainly to the X_1 and X_2 ground-state components. As already mentioned in the previous Section, the $v'=1$ vibrational levels of the A_1 and A_2 states are strongly predissociated due to spin–orbit interaction with the corresponding $^5\Sigma^-$ components.

Other possible candidates for the above experimental scheme lie much higher, at about $(53\text{ to }54)\cdot 10^3$ cm^{-1}, and belong to the first Rydberg $^3\Pi$ multiplet. They have very strong perpendicular transitions to the ground state, e.g., τ_p $(3\ ^3\Pi_2-X_2\ ^3\Sigma_1^-)\approx 12$ ns, and also quite strong transitions to the $a\ ^1\Delta$ state: $\tau_p\approx 5\ \mu$s. Similarly as for the $A\ ^3\Pi$ multiplet, experimental observation of the $3\ ^3\Pi$ state luminescence may be hampered because of its predissociation by the lower-lying valence states (see Figs. 4–7).

VI. CONCLUSION

Spin–orbit CI calculations based on relativistic effective core potentials have been employed to obtain potential-energy curves, dipole moments and radiative lifetimes for the low-lying valence and Rydberg states of the AsH radical. All electronic states which converge to the five lowest $\Lambda-S$ dissociation limits have been studied as well as many other strongly bound states going to the higher atomic asymptotes. As for all Group VA hydrides and halides, a low-energy electronic spectrum of AsH is determined primarily by the O_2-like π^2 states, $^3\Sigma^-$, $^1\Delta$, and $^1\Sigma^+$, plus the $\sigma\rightarrow\pi$ and $\pi\rightarrow\sigma^*$ $^{1,3}\Pi$ states. The lower-lying bound $\sigma\rightarrow\pi\ ^3\Pi$ state with an inverse order of Ω components distinguishes the hydride spectra from those of the halides, in which the $\pi^*\rightarrow\sigma^*\ ^3\Pi$ has a lower excitation energy.

There have been a number of thorough spectroscopic studies of the AsH radical and good agreement is found with the available experimental data. The present computed bond distances are slightly (by 0.01–0.02 Å) larger than the experimental values, which is probably due to the absence of an explicit treatment of the As atom $3d$ electrons in the computational approach employed. This effect is typical for all states considered, however, and thus should not influence the relative positions of these states. The corresponding computed vibrational frequencies are found to agree within 22 cm^{-1} of their observed values in all cases where such comparison is possible. Excitation energies for the singlet states, $a^1\Delta$ and $b^1\Sigma^+$, are slightly (by 450–550 cm^{-1}) overestimated in the present study, but a significant improvement is achieved with respect to the previous *ab initio* calculations, indicating a high level of the present correlation treatment.

The zero-field splittings are obtained quite accurately with the help of the As atom full-core RECP. This is true for the $X\ ^3\Sigma^-$ ground state and especially for the $A\ ^3\Pi$ multiplet. The present study confirms an experimental conclusion[3] that the $\Omega=0^-$, 1, and 2 components of the latter state are strongly predissociated due to spin–orbit interaction with the repulsive $^5\Sigma^-$ state. Generally speaking, spin–orbit interaction in the AsH radical is relatively weak, however, and as a result the lifetimes of most of the AsH low-lying states are quite long. For example, the $X_2\ ^3\Sigma_1^-$ state has an estimated lifetime of $\approx 6\cdot 10^5$ s, as compared to 16.1 ms for BiH. The corresponding $a^1\Delta$ values are 97 ms for AsH and 0.545 ms for the bismuth radical. The $b-X$ transition consists of two branches and the calculations show that the transition probability for the parallel component is much smaller than for the perpendicular. It is opposite to what was found earlier for the BiH radical[13] and is explained by a very small difference in the dipole moments of the $X\ ^3\Sigma^-$ and $b\ ^1\Sigma^+$ states from which the parallel $b-X_1$ transition mainly acquires its intensity. The total radiative lifetime of the $b\ ^1\Sigma^+$ state computed in the present study of 0.93 ms agrees well with the experimental estimate $\tau\geqslant 0.8$ ms.[29] The lifetimes of the $A\ ^3\Pi$ Ω components are considerably shorter than for any of the

lower-lying species, typically $\sim 1\ \mu$s for each of the A substates. This is a direct consequence of the fact that these transitions are dipole-allowed at the $\Lambda - S$ level of treatment. The $A\ ^3\Pi\Omega = 1$ and 2 components are good candidates for the LIF scheme for investigation of the $a\ ^1\Delta$ state, possessing fairly strong transitions for both the excitation $(A_{1,2} \leftarrow a)$ and fluorescence $(A_{1,2} \rightarrow X_{1,2})$ channels. By contrast, the $1\ ^1\Pi$ state is not suitable for this purpose since it has been calculated to be repulsive. The $2\ ^{3,1}\Pi$ states are probably also not interesting for the LIF experiments since they have minima significantly shifted to longer distances and are strongly predissociated due to numerous crossings with the lower-lying repulsive states.

At energies higher than $53 \cdot 10^3\ \mathrm{cm}^{-1}$ numerous Rydberg states appear which arise from the $\sigma,\ \pi \rightarrow \sigma_R,\ \pi_R$ excitations. They are strongly bound and characterized by much more intense transitions to the ground state than any of the valence states discussed above. A good example of such a radiative process is provided by the $3\ ^3\Pi_{0^+} \rightarrow X_2\ ^3\Sigma_1^-$ transition, with a τ_p value estimated to be 12 ns. No experimental observations of these states have been reported to date, and we hope that the present calculated data may stimulate future spectroscopic study.

ACKNOWLEDGMENTS

The authors are very grateful for numerous discussions with Professor E. H. Fink and Dr. O. D. Shestakov during the course of the present study. This work was supported in part by the Deutsche Forschungsgemeinschaft in the form of a Forschergruppe grant and within the Schwerpunktprogramm Theorie relativistischer Effekte in der Chemie und Physik schwerer Elemente. The financial support of the Fonds der Chemischen Industrie is also hereby gratefully acknowledged.

[1] M. Beutel, K. D. Setzer, O. Shestakov, and E. H. Fink, J. Mol. Spectrosc. **178**, 165 (1996).
[2] R. N. Dixon, G. Duxbury, and H. M. Lamberton, Chem. Commun. **14**, 460 (1966).
[3] R. N. Dixon and H. M. Lamberton, J. Mol. Spectrosc. **25**, 12 (1968).
[4] K. Kawaguchi and E. Hirota, J. Mol. Spectrosc. **106**, 423 (1984).
[5] J. R. Anacona, P. B. Davies, and S. A. Johnson, Mol. Phys. **56**, 423 (1984).
[6] K. D. Hensel, R. A. Hughes, and J. M. Brown, J. Chem. Soc. Faraday Trans. **91**, 2999 (1995).
[7] M. Arens and W. Richter, J. Chem. Phys. **93**, 7094 (1990).
[8] J. Berkowitz, J. Chem. Phys. **89**, 7065 (1988).
[9] L. G. M. Pettersson and S. R. Langhoff, J. Chem. Phys. **85**, 3130 (1986).
[10] T. Matsushita, C. M. Marian, R. Klotz, and S. D. Peyerimhoff, Can. J. Phys. **65**, 155 (1987).
[11] K. Balasubramanian, J. Chem. Phys. **91**, 2443 (1989).
[12] K. Balasubramanian and V. Nannegari, J. Mol. Spectrosc. **138**, 482 (1989).
[13] A. B. Alekseyev, R. J. Buenker, H.-P. Liebermann, and G. Hirsch, J. Chem. Phys. **100**, 2989 (1994).
[14] H.-P. Liebermann, I. Boustani, S. N. Rai, A. B. Alekseyev, G. Hirsch, and R. J. Buenker, Chem. Phys. Lett. **214**, 381 (1993).
[15] A. B. Alekseyev, A. B. Sannigrahi, H.-P. Liebermann, R. J. Buenker, and G. Hirsch, J. Chem. Phys. **103**, 234 (1995).
[16] M. M. Hurley, L. F. Pacios, P. A. Christiansen, R. B. Ross, and W. C. Ermler, J. Chem. Phys. **84**, 6840 (1986).
[17] T. H. Dunning, Jr., J. Chem. Phys. **35**, 716 (1971).
[18] C. E. Moore, Arch. U. S. Natl. Bur. Stand. No. **467**, Vol. 3 (1971).
[19] R. J. Buenker and S. D. Peyerimhoff, Theor. Chim. Acta **35**, 33 (1974); **39**, 217 (1975); R. J. Buenker, S. D. Peyerimhoff, and W. Butscher, Mol. Phys. **35**, 771 (1978).
[20] E. R. Davidson, in *The World of Quantum Chemistry*, edited by R. Daudel and B. Pullman (Reidel, Dordrecht, 1974), p. 17.
[21] G. Hirsch, P. J. Bruna, S. D. Peyerimhoff, and R. J. Buenker, Chem. Phys. Lett. **52**, 442 (1977); D. B. Knowles, J. R. Alvarez-Collado, G. Hirsch, and R. J. Buenker, J. Chem. Phys. **92**, 585 (1990).
[22] R. J. Buenker and R. A. Philips, J. Mol. Struct.: THEOCHEM **123**, 291 (1985).
[23] A. B. Alekseyev, H.-P. Liebermann, R. J. Buenker, G. Hirsch, and Y. Li, J. Chem. Phys. **100**, 8956 (1994).
[24] R. J. Buenker, A. B. Alekseyev, H.-P. Liebermann, R. M. Lingott, and G. Hirsch, J. Chem. Phys. (to be published).
[25] J. W. Cooley, Math. Comput. **15**, 363 (1961).
[26] M. Perić, R. Runau, J. Römelt, S. D. Peyerimhoff, and R. J. Buenker, J. Mol. Spectrosc. **78**, 309 (1979).
[27] C. Zetzsch, Ber. Bunsenges. Phys. Chem. **82**, 639 (1978).
[28] K. K. Das, A. B. Alekseyev, H.-P. Liebermann, G. Hirsch, and R. J. Buenker, Chem. Phys. **196**, 395 (1995).
[29] E. H. Fink, K. D. Setzer, and O. Shestakov (private communication).